Applied Catalysis A: General 375 (2010) 188-195

Catalytic characterization of pure SnO_2 and GeO_2 in methanol steam reforming

Q. Zhao[1], H. Lorenz[1], S. Turner[2], O. I. Lebedev[2], G.Van Tendeloo[2], C. Rameshan[1,3], B. Klötzer[1], J. Konzett[4], S. Penner[1,*]

[1]Institute of Physical Chemistry, University of Innsbruck, A-6020 Innsbruck, Austria
[2]EMAT, University of Antwerp, B-2020 Antwerp, Belgium
[3]Department of Inorganic Chemistry, Fritz-Haber Institute of the Max-Planck Society, D-14195, Berlin, Germany
[4]Institute of Mineralogy and Petrography, University of Innsbruck, A-6020 Innsbruck, Austria

[*] Corresponding author: e-mail simon.penner@uibk.ac.at,

Received: 21 October 2009; Received in revised form 7 December 2009; Accepted 17 December 2009
Available online 13 January 2010

Abstract

Structural changes of a variety of different SnO, SnO_2 and GeO_2 catalysts upon reduction in hydrogen were correlated with associated catalytic changes in methanol steam reforming. Studied systems include SnO, SnO_2 and GeO_2 thin film model catalysts prepared by vapour phase deposition and growth on polycrystalline NaCl surfaces and, for comparison, the corresponding pure oxide powder catalysts.

Reduction of both the SnO_2 thin film and powder at around 673 K in 1 bar hydrogen leads to a substantial reduction of the bulk structure and yields a mixture of SnO_2 and metallic β-Sn. On the powder catalyst this transformation is fully reversible upon oxidation in 1 bar O_2 at 673 K. Strongly reduced thin films, however, can only be re-transformed to SnO_2 if the reduction temperature did not exceed 573 K. For GeO_2, the situation is more complex due to its polymorphism. Whereas the tetragonal phase is structurally stable during reduction, oxidation or catalytic reaction, a small part of the hexagonal phase is always transformed into the tetragonal at 673 K independent of the gas phase used.

SnO_2 is highly active and CO_2-selective in methanol steam reforming, but the initial high activity drops considerably upon reduction between 373 and 573 K and almost complete catalyst deactivation is observed after reduction at 673 K, which is associated with the parallel formation of β-Sn. In close correlation to the structural results, the catalytic activity and selectivity can be restored upon an oxidative catalyst regeneration at 673 K. Tetragonal GeO_2 exhibits only a small activity and no pronounced selectivity to either CO or CO_2, at least after reduction. In its fully oxidized state release of surface/lattice oxygen results in a non-catalytic formation of CO_2 by oxidation of CO originating from catalytic dehydrogenation.

Keywords: Electron Microscopy, EELS, SnO_2, SnO, GeO_2, methanol steam reforming, CO_2 selectivity

1. Introduction

The interest in SnO_2 as a heterogeneous catalyst is mainly driven by its capability to act as an efficient oxidation catalyst, especially in reactions involving CO [1]. Most of these reactions are explained by a Mars-van-Krevelen-type reaction mechanism, that is, by the involvement of lattice oxygen, whereby the created oxygen vacancy is subsequently replenished by oxygen from the gas phase. Hence, the central issue in catalytic discussions involving SnO_2 is its easy reducibility, giving rise to the presence of Sn^{4+} and Sn^{2+} surface sites during a catalytic cycle. This is also of special importance in view of the recently discovered ability of SnO_2 to steer the steam reforming of methanol to CO_2, since the adsorption of the steam reforming reactants is reported [1] to be significantly influenced by the ratio of Sn^{4+} to Sn^{2+}, that is, the reduction degree of SnO_2. Concerning methanol dissociation on SnO_2 (110) surfaces, the conversion rate of methanol to formaldehyde was observed to be strongly dependent on the reduction degree of the surface with diminished reactivity of the initially active four-fold coordinated Sn^{2+} sites after further

reduction of the surface [1]. For water adsorption and dissociation a strong dependence on sample pre-treatments, and hence, the presence of oxygen vacancies and related surface defect sites, was observed [1]. It was also reported that the presence of water significantly inhibits the reduction of SnO_2 to metallic Sn [2].

The interest to include SnO_2 and GeO_2 in studies on methanol steam reforming in more detail is additionally derived from the properties of previously studied oxides such as ZnO [3], Ga_2O_3 [4] or In_2O_3 [5]. The main feature of all these oxides is their role as supports and/or catalysts in methanol steam reforming, but, depending on the surface chemistry and redox properties, the desired selectivity to CO_2 varies. Pure In_2O_3 is highly CO_2-selective, both ZnO and Ga_2O_3 are not [4,6]. Partly this is also due to their activity in the reverse water-gas shift reaction [7,8]. From a chemical analogy argument, Sn^{4+} and In^{3+} represent isoelectronic species and therefore we may speculate about a potential functional analogy of their catalytic action. The same holds for Ge^{4+}, Ga^{3+} and Zn^{2+}, which renders an extension of the studies to the fourth main group of the periodic system useful. Information on the catalytic properties of GeO_2 is scarce and is mainly limited e.g. to the use of GeO_2 as a promoter in the selective hydrogenation of nitric acid or the use of bimetallic Pt and Rh-Ge particles in hydrogenation reactions [9].

On the basis of the structural results of the thin film model preparation discussed in a separate publication [10], the present contribution therefore is focussed on the structural changes of the SnO_2 and GeO_2 thin films upon reduction and the subsequent correlation to catalytic activity and selectivity in methanol steam reforming. The thin film model approach is especially suited for combining structural characterization of well-defined and ordered oxide particles by (HR)TEM with catalytic characterization in a dedicated microreactor setup to result in unambiguous structure-activity correlations. To close the materials gap to more "real" catalysts, special attention will also be paid to the comparison of thin films with the respective oxide powder samples and to the general correlation of the results to those obtained on the corresponding oxides in the 3rd main group of the periodic system, namely Ga_2O_3 and In_2O_3 [4,5]. A short resume of the most important results of catalyst preparation will precede the results section of this paper.

2. Experimental

SnO and GeO_2 films were prepared by reactive deposition of thermally evaporated SnO_2 (Alfa Aesar, 99.999%) in10^{-3} mbar O_2 or GeO_2 (Alfa Aesar 99.9999%, α-quartz-type with hexagonal structure) in 10^{-4} mbar O_2 at varying substrate temperatures (300 K-600 K) (thickness of the support 25 nm each) onto NaCl(001) cleavage faces (TEM samples) or freshly deposited NaCl films (catalytic samples, about 37 cm^2). The latter are necessary for the catalyt

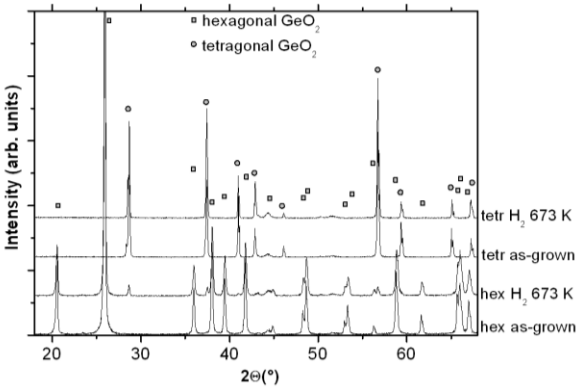

Fig. 1: Set of XRD spectra of the hexagonal and tetragonal GeO_2 phase in the initial state and after reduction

ic experiments to obtain sufficiently high conversion rates. The structural identity of films grown on single-crystalline NaCl(001) and polycrystalline NaCl films has been outlined in a number of publications [5]. All films used for catalytic experiments were subsequently covered by a layer of amorphous SiO_2 (prepared by reactive deposition of SiO in 10^{-4} mbar O_2 at 300 K) to improve the mechanical stability (mean SiO_2 thickness 1000 nm). The films were thoroughly rinsed with distilled water, dried and finally mounted on quartz wool inside the reactor or on gold grids for electron microscopy. The SnO (Alfa Aesar, 99.9%) and SnO_2 powder samples were used as such. Due to the polymorphism of GeO_2 [11], extra care had to be taken upon characterizing the GeO_2 powder samples. As in principle two phases, a hexagonal α-quartz type structure and tetragonal rutile-type structure are stable at room temperature [11], phase purity of the catalyst samples is crucial. In our context this essentially refers to structural transitions during catalyst activation treatments. This issue will be addressed in detail in section 3.4. Figure 1 shows an overview of X-ray diffraction (XRD) spectra of both polymorphs in the as-grown state, among others. The rutile-type phase is usually prepared starting from the widespread commercially available hexagonal phase by a complex dissolution-precipitation procedure using e.g. ammonium fluoride as a precipitation aid to form the structural precursor of the tetragonal phase and to suppress the precipitation of the (slightly water-soluble) hexagonal phase *or* alternatively by a structural transformation at high pressures and temperatures, according to the Ge-O phase diagram [11-13]. In our case, tetragonal GeO_2 was synthesized from high purity (99.9999%) hexagonal GeO_2 in a gold capsule at 2000 bars and 1000 K using a cold-seal pressure vessel. The duration of the synthesis experiment was 48 hours. This procedure transforms the hexagonal phase quantitatively into the tetragonal phase, as verified by XRD (see Fig.1) and Raman spectroscopy. All powder samples were subjected to analogous treatments to ensure an unambiguous correlation to the thin film samples.

Catalytic measurements in methanol steam reforming as well as catalyst activation treatments of *all* samples were performed in an NI Labview-automatized recirculating batch reactor of about 8 ml volume [14]. The system allows automated pre-treatment cycles (oxidative and reductive) and reaction sequences. Both thin films and powder samples were subjected to annealing treatments in either hydrogen or oxygen as high as 673 K (1 bar, 1h each).

The catalytic measurements were performed using a quadrupole mass spectrometer (Balzers QMG 311) attached to the circulating batch Duran glass reactor via a capillary leak. All methanol steam reforming reactions were conducted with methanol/water mixtures of a 1:9 composition of the liquid phase at room temperature. The gas phase compositions of a variety of different liquid mixtures have been empirically determined by mass spectrometry. On the basis of these measurements we could derive that the volumetric 1:9 mixture corresponds to a gas phase composition of 1:2 = methanol:water at room temperature. All methanol/water mixtures were degassed by repeated freeze-and-thaw cycles. For each catalytic methanol steam reforming experiment, to about 5 mbar methanol/water mixture, 7.5 mbar Ar (to be measured at m/z = 40) was added to account for the decrease of the mass spectrometer signal due to the continuous gas withdrawal through the leak. Finally, He was added to 1 bar total pressure.

The molecular masses m/z =2 (H_2), 16 (CH_4), 18 (H_2O), 28 (CO/N_2), 29 ($CH_3OH/HCOOH$), 30 (CH_2O), 31 (CH_3OH/CH_2O), 32 (CH_3OH/O_2), 40 (Ar) and 44 (CO_2), 45 (HCOOH) and 46 (HCOOH) were routinely collected. All mass spectrometer signals of CH_3OH, CO_2, CO, and H_2 were externally calibrated and corrected for fragmentation in the mass spectrometer. This includes m/z = 28 for both CO_2 and CH_3OH and m/z = 45 for CO_2. In order to account for the partial adsorption of methanol and water on the stainless steel parts of the reaction system, all catalytic measurements include a 15 minute equilibration period in the starting mixture prior to each measurement. For methanol steam reforming, both temperature-programmed conversion and conversion versus time under isothermal conditions were monitored. In each case, the catalyst was exposed to the reaction mixture and the temperature was ramped with 5 K/min to the final value. For the partial pressure change versus time experiments, the product formation was monitored for 1 hour each at fixed reaction temperature. All the catalytic experiments were also corrected for the activity of the catalyst holder containing only quartz wool (almost negligible, at maximum 1 % conversion based on CO_2 formation after 1 h). For data evaluation, the relative intensities of the mass spectrometer signals were converted into partial pressures via external calibration using gas mixtures of defined partial pressures. For clarity, all catalytic results are usually plotted as partial pressure change versus temperature or time.

Overview TEM imaging and Selected Area Electron Diffraction (SAED) were carried out with a ZEISS EM10C microscope, Electron-Energy Loss Spectroscopy (EELS) was performed on a JEOL 3000F FASTEM microscope operated at 300 kV and equipped with a GIF 2000 post-column electron energy-loss spectrometer. The film composition was checked by Energy-dispersive X-ray Analysis (EDXS), which only showed peaks due the evaporated elemental thin film constituents (Sn, Ge and O) and the gold grid (Au). Surface carbon impurities present on the films were removed by Ar-sputtering prior to TEM imaging. No influence of the sputtering on structure and morphology of the films has been detected. The purity of the substrate was ensured by freshly cleaving the NaCl(001) crystals immediately before deposition of the oxide. The SAED patterns were calibrated with respect to SnO spots in the untreated, as-grown state of the catalyst deposited in 10^{-3} mbar O_2 at 473 K.

X-ray diffraction experiments were performed ex-situ under ambient conditions using a Siemens D5000 Spectrometer and Cu-K_α radiation (1.54178 Å) at 300 K.

3.Results and Discussion

3.1. Preparation and characterization of SnO_x and GeO_2 thin film model catalysts

SnO_x films exhibit a 1:1 stoichiometry of Sn:O after deposition in 10^{-3} mbar O_2 at 473 K as evidenced by electron diffraction. Lower oxygen partial pressures lead to formation of β-Sn particles within the SnO matrix, for higher oxygen partial pressures no reproducible evaporation rates could be obtained due to oxidative inhibition of the formation of volatile SnO_x gas phase species. SnO_2 films are therefore prepared by post-oxidation of the SnO films at 673 K in 1 bar O_2 for 1h. The grain structure of both crystalline films is similar and consists of round-shaped grains of about 10 nm.

Preparation of GeO_x films always yields amorphous films with a composition close to GeO_2, which resist crystallization or decomposition by annealing treatments in oxygen or hydrogen at temperatures comparable to SnO/SnO_2. Details are given elsewhere [10].

3.2. Structural characterization of the SnO and SnO_2 powder and thin film catalysts upon reduction

Since the thin films deposited at 473 K yielded the best-crystallized and ordered SnO films, all the catalytic films of SnO (and SnO_2 after post-oxidation of these films at 673 K) discussed below are prepared this way. Representative XRD spectra of the starting SnO_2 and SnO powders (Figure 2) correspond to the tetragonal rutile-type α-SnO_2 phase and the tetragonal PbO-type SnO phase [15,16]. As additional spectroscopic information, and also as a reference for subsequent reduction experiments, Figure 3 highlights representative energy loss near-edge structures (ELNES) of Sn-$M_{4,5}$ and O-K edges of the SnO_2 and SnO

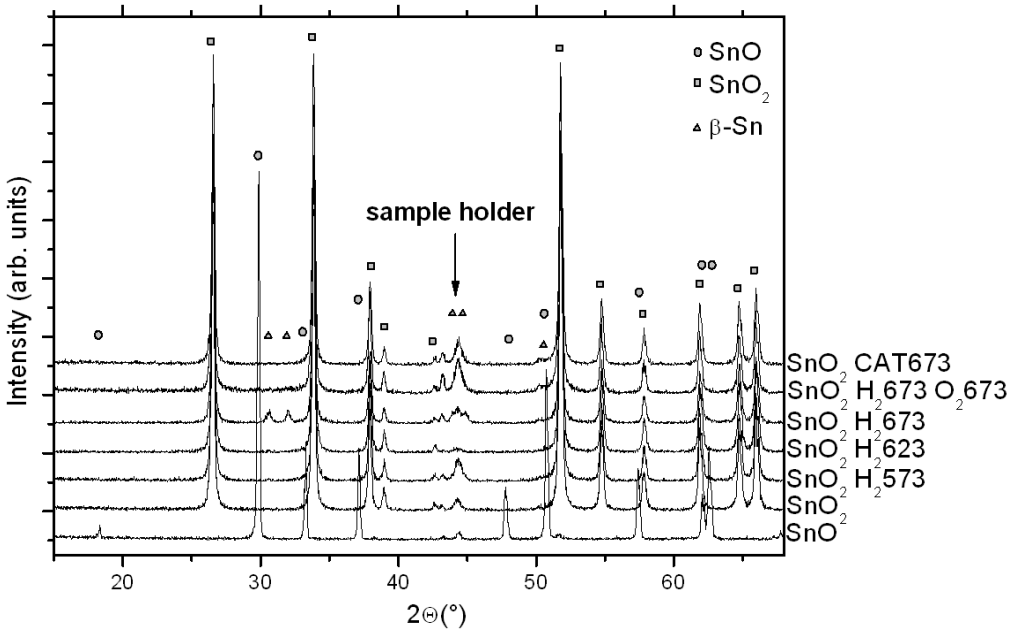

Fig. 2: Set of XRD spectra of the initial SnO and SnO_2 phases and after different activation treatments

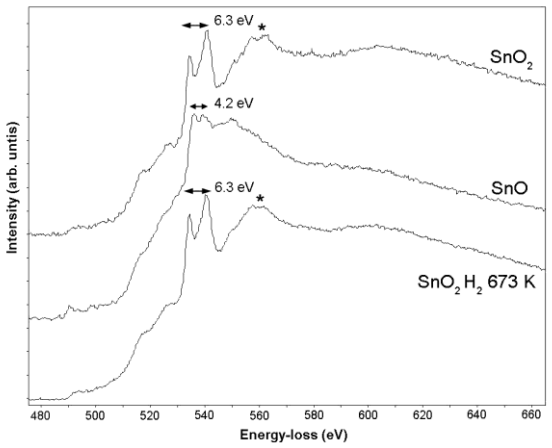

Fig. 3: Electron-energy loss spectra (Sn-$M_{4,5}$ and O-K edges) of the initial SnO and SnO_2 powders and after reduction of SnO_2 at 673 K.

powders in the initial states and after reduction at 673 K. Both the SnO_2 and SnO edges agree well with literature-reported spectra and also with EELS spectra taken on the respective thin films after preparation at 473 K in 10^{-3} mbar O_2 (SnO) and after post-oxidation in O_2 at 673 K (SnO_2) [10,17]. After reduction at 673 K, the EELS spectra still resemble the shape of SnO_2, although formation of a small quantity of metallic β-Sn has been observed in the XRD pattern (See Figure 2 and discussion below).

Figure 4 highlights the structural evolution of a SnO_2 film upon treatment in hydrogen at 473 K (a), 573 K (b) and 673 K (c). The overview electron micrographs taken after reduction at 473 K and 573 K reveal no substantial morphological changes as compared to the fully oxidized state. The porous grain structure typical for both SnO and SnO_2 still persists. However, in the corresponding SAED patterns (Figure 4d and e) rather strong reflections of the SnO structure reappear at 473 K reduction temperature and get more pronounced at 573 K. At this temperature, no more reflections of the tetragonal SnO_2 structure are visible. However, a pronounced structural transformation has been observed after reduction at 673 K. Figure 4c reveals that some patches of the former SnO structure still remain, but the structure is dominated by very large, oval-shaped particles, which are obviously formed by coalescence of highly mobile smaller particles. In the corresponding SAED patterns the tetragonal SnO phase is still detectable, but additional ring reflections at 2.9 Å, 2.8 Å, 2.1 Å and 2.0 Å appear. These can be attributed to the (200), (101), (220) and (211) reflections of the cubic structure of β-Sn [$d_{theor}(200)$ = 2.9158 Å, $d_{theor}(101)$ = 2.7928 Å, $d_{theor}(220)$ = 2.0618 Å and $d_{theor}(211)$ = 2.0169 Å] [18]. The epitaxy and crystallinity of the SnO phase has been observed to crucially influence the reduction behaviour of the films, that is, if a SnO film was prepared at 300 K in 10^{-3} mbar O_2 (which only yields an initially amorphous SnO phase), and thereafter reduced at 673 K, a substantial reduction to β-Sn has been observed *without* any crystallization of SnO. The reduction of the corresponding SnO_2 powder sample is shown as a set of XRD spectra in Figure 2. Up to reduction tem

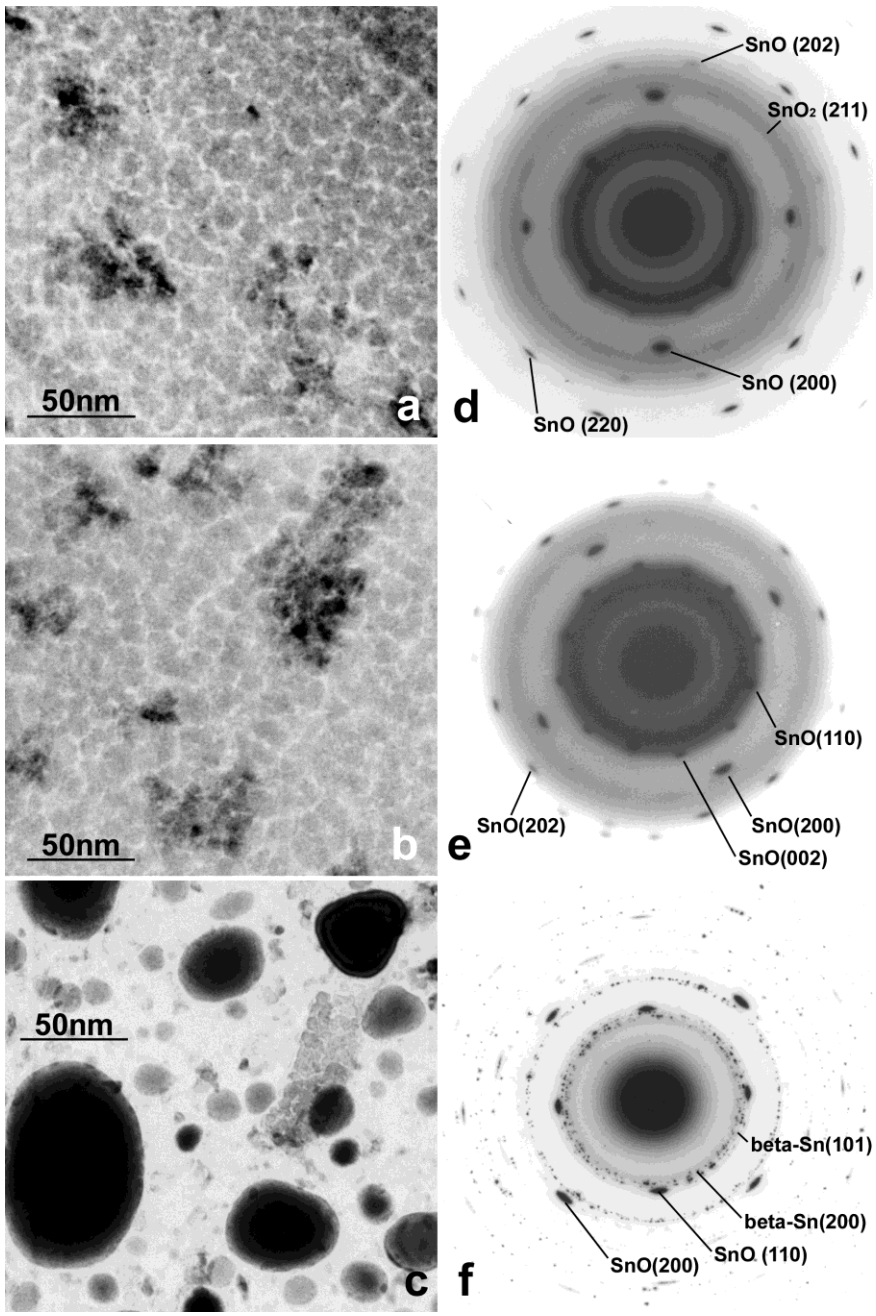

Fig. 4: TEM micrographs of the structural evolution of SnO_2 thin films after reduction in hydrogen at 473 K (a), 573 K (b) and 673 K (c). The corresponding SAED patterns are shown in (d)-(f).

peratures of 623 K, tetragonal SnO_2 is the only structure observed. Additional peaks, which can be attributed to the β-Sn phase, only appear at 673 K. It is worth noting that during the entire reduction phase - also at lower reduction temperatures - detectable bulk amounts of crystalline SnO have never been detected. For the sample reduced at 673 K, this is evident by comparison with the bottom-most XRD spectrum, denoting the reference SnO powder. This behaviour agrees well with previous studies on the reduction of SnO and SnO_2 by molecular hydrogen. Below about 673 K (the disproportionation temperature of SnO), SnO_2 was reported to be reduced to metallic Sn via intermediary formed SnO. The situation at lower annealing/reduction temperatures is complicated by the dependence of SnO on annealing and reduction properties. SnO disproportionates into SnO_2 and Sn upon annealing under equilibrium conditions, but the stability limit was observed to be strongly dependent on the annealing conditions and sample pretreatment and preparation. Powder SnO was reported to be reduced in hydrogen to metallic tin at around 473 K [19].

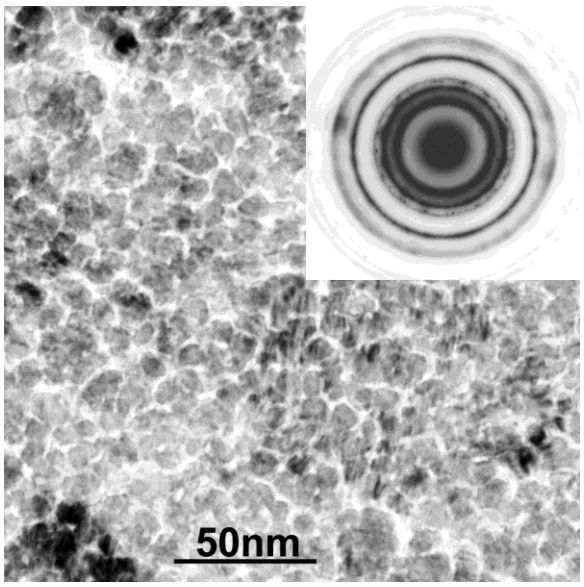

Fig. 5: TEM micrograph of the SnO_2 film shown in Figure 4b after oxidation at 673 K. The SAED pattern is shown as inset.

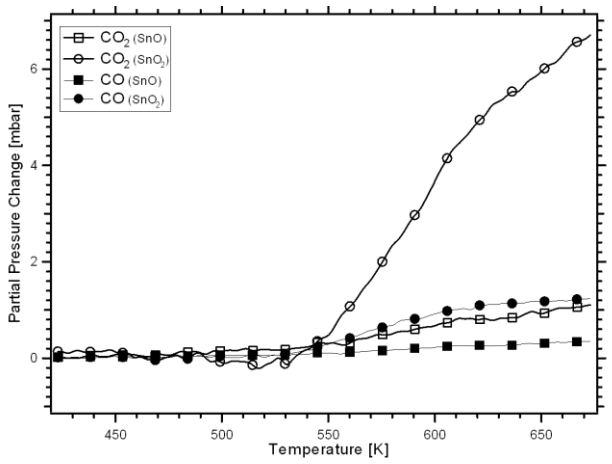

Fig. 6: Methanol steam reforming reaction over the initial, untreated SnO_2 (circles) and SnO (squares) powders.

3.3. Oxidative catalyst regeneration

A question of crucial importance for all catalytic experiments is related to catalyst regeneration. Since a calcination cycle in the present case involves both oxidation and reduction treatments also at elevated temperatures, it is inevitable to ensure that all structural and compositional changes are fully reversible. Figure 5 shows that it is indeed possible to reconvert any changes that have been introduced to the SnO/SnO_2 thin films by reduction at temperatures $T \leq 573$ K by simple re-oxidation at 673 K in 1 bar O_2 (1 h). Both the electron micrographs and the SAED pattern are typically for SnO_2 and are indistinguishable from patterns obtained by simple post-oxidation of single-crystalline SnO films. The same holds for the SnO_2 powder. The second spectrum from the top in Figure 2, collected after re-oxidation of the powder pre-reduced at 673 K also at 673 K (1 bar O_2, 1 h), shows no signs of metallic Sn or tin oxides with Sn in lower oxidation states. The top-most spectrum reveals that no substantial structural or compositional changes are expected after exposing the SnO_2 powder to a catalytic mixture of 50 mbar methanol/water (He added to 1 bar total pressure) at temperatures as high as 673 K (these are the highest reaction temperatures that are applied in subsequent catalytic reactions. Typically, methanol steam reforming reactions are not run at higher temperatures than 623-673 K). Similar observations have been made on the respective thin film catalysts and for the tetragonal GeO_2 samples (thin film and powder; for hexagonal GeO_2 the situation is more complex, see section 3.4.). This also agrees well with studies of Morikawa et al. on methanol steam reforming on SnO_2, who also observed that water suppresses the formation of metallic tin during reduction in hydrogen [2]. This indicates that water is able to adsorb on oxygen vacancies of SnO_2 formed during the reduction and effectively quenches the vacancies by replenishment of lattice oxygen.

3.4. Structural characterization of the GeO_2 catalysts upon reduction

Oxidative and reductive treatments in O_2 or H_2 at temperatures as high as 673 K do not change the film structure or cause crystallization of previously amorphous films. As already indicated in section 2, the structural characterization of the GeO_2 powder sample is complicated by the polymorphism of GeO_2. The XRD spectra shown in Figure 1 also reveal that after reduction at 673 K, a small part of the original hexagonal GeO_2 phase is transformed into the tetragonal structure. In contrast, the tetragonal phase remains phase-pure after a similar treatment in hydrogen. This behaviour is not entirely clear, but seems to be a thermal annealing phenomenon, since it also happens - independently of the gas phase used - at 673 K. It also agrees well with studies of Bertini et al. [20] who obtained a complete transformation into the tetragonal phase by simple annealing the hexagonal phase at 1023 K for 700 h. Possible consequences of this structural behaviour for the catalytic properties will be dealt with in the following section.

3.5. Catalytic characterization in methanol steam reforming

On the basis of previous studies by Morikawa et. al. on the use of SnO_2 as a CO_2-selective methanol conversion and methanol steam reforming (MSR) catalyst [2], we especially focussed in the following on the catalytic characterization of SnO and SnO_2 and the influence of reductive pre-treatments on catalytic activity and selectivity. A correlation to GeO_2 and previously studied oxides of the 3rd main group of the periodic table will be discussed.

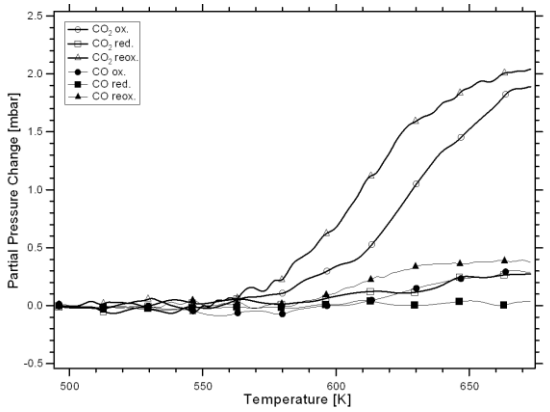

Fig. 7: Methanol steam reforming reaction over the initial SnO_2 thin film (circles), after reduction at 573 K (squares) and after subsequent oxidation at 673 K (triangles).

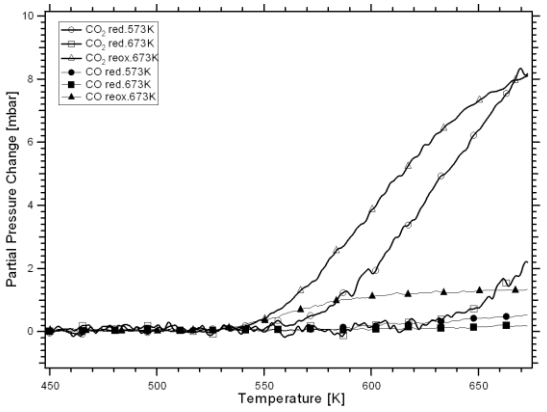

Fig. 8: Methanol steam reforming reaction over the SnO_2 powder reduced at 573 K (circles), after reduction at 673 K (squares) and after subsequent oxidation at 673 K (triangles).

Figure 6 highlights the temperature-programmed MSR reaction over pure SnO_2 and SnO powder catalysts (BET surface areas 7 m^2/g and 0.4 m^2/g, respectively; for a better comparison, the masses of both catalysts were chosen to result in the same total surface area of ~ 0.1m^2). Reaction over SnO_2 starts at around 530 K, which is comparable to In_2O_3 [5], but much less compared to Ga_2O_3 (600 K) [4]. A strong acceleration of the CO_2 formation was observed between 550 and 670 K; at higher reaction temperatures only slight catalyst deactivation is observed. Apart from CO_2, CO is the other main product formed (at maximum ~14 % at 673 K). The product mixture at the end of the reaction at 673 K was routinely analyzed by gas chromatography coupled with mass spectrometry (GC-MS), but in contrast to Morikawa et al., who reported methane amounts of as high as 10% [2] (and only trace amounts of CO of around 1% at 623 K; detection mode gas chromatography with thermal conductivity/flame ionization detector), only minor amounts of methane were observed in our case (less than 1% at the highest reaction temperatures). To clarify this discrepancy, methane was deliberately added to the reaction mixture (~3 mbar) and the methanol steam reforming reaction performed under otherwise identical conditions, in order to determine if methane is consumed during the reaction in the batch reactor. After analyzing the reaction mixture at 673 K by GC/MS, no significant methane consumption and/or additional formation was found. The CO/CO_2 product selectivity very much resembled the one without methane. We hence conclude that methane is neither a reaction product nor an intermediate species which is consumed in the course of the reaction in the batch reactor. Methanol steam reforming over an SnO powder catalyst (filled circles and squares) yielded a much lower overall conversion of methanol as compared to SnO_2 (approximately 20% total conversion; almost 100% conversion was measured on SnO_2). CO_2 appears to be the main product with CO being the most notable by-product.

A qualitatively very similar reaction selectivity pattern has been obtained on the respective thin film model catalysts. Figure 7 highlights the MSR reaction over the thin films prepared at 473 K in 0.1 Pa O_2 and subsequently oxidized at 673 K (i.e. SnO_2, circles) and thereafter reduced at 573 K (i.e. SnO, squares). A correlation to the powder catalysts can therefore be easily obtained. CO_2 is the main product (selectivity about 85%), with CO being the most notable by-product and the SnO phase is again much less active than SnO_2.

The influence of catalyst reduction on the SnO_2 powder is shown in Figure 8. By comparison with Fig. 6 denoting the MSR reaction over fully oxidized SnO_2, it is clear that after reduction at 573 K (no additional signals visible in the XRD pattern-Fig.2) the catalytic activity already drops by a factor of two. After reduction at 673 K, the catalyst is almost deactivated and only a small amount of CO_2 is formed. Since no SnO is detected at any of these reduction stages and scanning electron micrographs (not shown) do not indicate a considerable sintering upon reduction, the loss of activity can be attributed to the formation of a surface SnO coating preceding the reduction to metallic tin at higher reduction temperatures.

In close correlation to the structural regeneration of both powder and thin film catalysts highlighted in Figures 2 and 5, both SnO_2 catalysts were subjected to oxidative treatments at 673 K after pre-reduction and subsequently examined in MSR. The corresponding reaction profiles shown in Figure 7 and 8 (triangles) reveal that indeed also the catalytic activity can be almost fully restored after a reduction at 673 K (powder) and 573 K (thin films). Higher reduction temperatures were not examined for the thin films since structural film destruction starts after reduction at 673 K (see Fig. 4c).

As for all the other oxides discussed in view of their methanol steam reforming activity/selectivity, the catalytic properties of SnO_2/SnO are crucially influenced by their surface chemistry. Both SnO and SnO_2 are amphoteric oxides [21]; according to a scheme of Tatibouet related to the product selectivity in methanol oxidation using molecular O_2, depending on the acid-base properties of the respective oxidic surface sites [22], this should primarily lead to

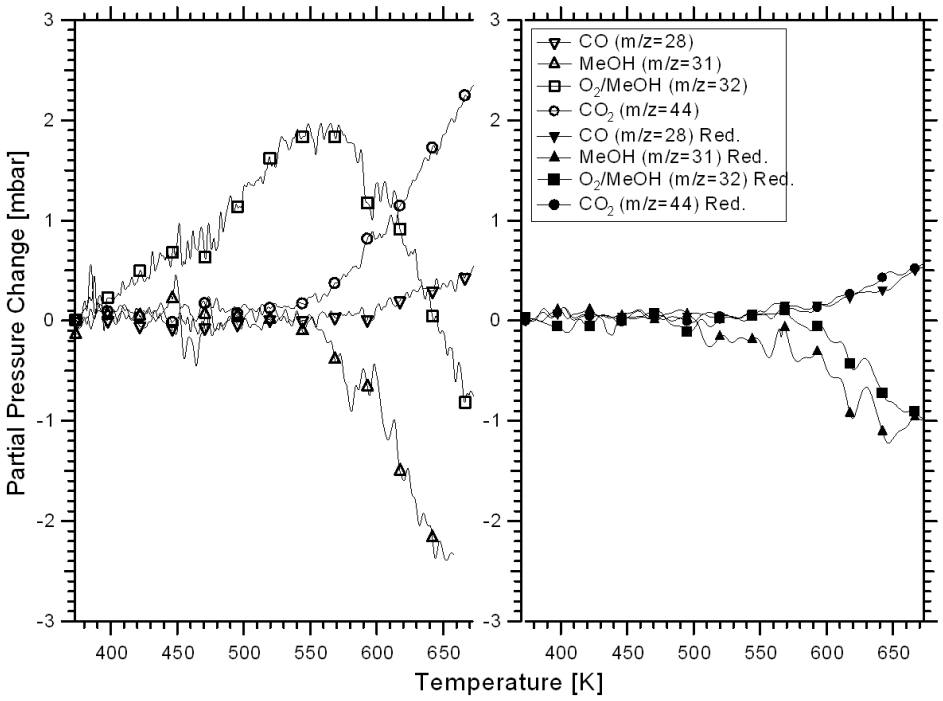

Fig. 9: Methanol steam reforming reaction over the tetragonal GeO_2 powder oxidized at 673 K in 1 bar O_2 for 1 h (left panel) and reduced at 473 K in 1 bar H_2 for 1 h (right panel).

partially oxidized products like formaldehyde, formic acid or formic acid methyl ester. Carbon oxides are more selectively formed in the presence of oxygen only over oxides with pronounced basic character [22]. Badlani et al., also using molecular O_2, reported the exclusive formation of partial oxidation products over SnO_2 catalysts, namely formaldehyde and formic acid methyl ester [23]. The present results for methanol steam reforming, in agreement with Moriwaka et al. [2], however indicate fast total oxidation of intermediate oxygenates to CO_2 and CO. A combination of the presence of a sufficiently high water partial pressure and highly efficient water activation at vacancy sites of SnO_2 may explain this discrepancy.

GeO_2 was already tested upon an extended screening of various oxides in methanol oxidation. It, however, was reported that it did not show a considerable conversion between 373 and 773 K, which was attributed to the low surface area of the respective sample [23]. Generally, GeO_2 is an amphoteric oxide with more acidic character [21]. According to the concept of Tatibouet, this should lead to "dehydration" products, such as dimethylether or dimethoxymethane (the latter requires one oxidation step before dehydration), since transformation and oxidation of the adsorbed methoxy group is largely suppressed. In the presence of a sufficiently high water partial pressure, dehydration reactions are likely to be suppressed.

Figure 9 highlights the methanol steam reforming reaction over fully oxidized (1 bar O_2, 673 K, left panel)) and reduced (1 bar H_2, 473 K, right panel) tetragonal GeO_2. After both treatments, the reaction starts at around 550 K, as deduced from the decrease of the methanol signal (m/z = 31). Along with this decrease goes a slight increase in the CO signal. Major differences in the MSR reaction between the two treatments are noted in the m/z = 32 (methanol/O_2) and m/z = 44 (CO_2) signals. On the fully oxidized system, the m/z =32 signal rises continuously between 373 and 550 K and drops sharply at higher temperatures, in parallel with the m/z = 31 methanol signal. This drop goes also along with an increase in the CO_2 signal. After reduction, both the m/z =31 and 32 traces decrease in parallel at 550 K. CO and CO_2 are formed in almost equal, but only small amounts. The question now arises where the maximum in the m/z = 32 signal comes from. To clarify this issue, pure tetragonal GeO_2 was heated after oxidation at 673 K in clean He up to 673 K and the m/z = 32 signal detected by MS. In short, a continuous increase in the signal was observed between 373 and 673 K (not shown), which indicates, that oxygen is easily released from the fully oxidized rutile-type surface/lattice upon heating. In turn, a part of the CO formed in the meanwhile is converted into CO_2 at somewhat higher temperature, causing the observed decrease. No such behaviour has been observed on the reduced surface. We tentatively interpret this peculiar phenomenon by a more substantial reduction of the GeO_2 surface/lattice after reduction in hydrogen at 473 K and subsequently, no more weakly bound oxygen is released during the MSR reaction between 373 and 673 K. It is, however, worth to note, that the reaction profile after reduction is quite similar to Ga_2O_3 and also indicates fast oxidation of the intermediate oxygenate species. The hexagonal GeO_2 phase was not considered for evaluation in the MSR reaction, since during the reaction a part of the hex-

agonal phase (as in hydrogen and oxygen atmospheres) is converted into the tetragonal phase and phase purity could not be guaranteed.

4. Conclusions

We demonstrated the catalytic activity and selectivity of SnO_2 and GeO_2 in methanol steam reforming, in close correlation to the already studied oxides in the 3rd main group of the periodic system, namely Ga_2O_3 and In_2O_3 [4,5]. Based on the assumption of a potential functional analogy of the catalytic action of the isoelectronic $Zn^{2+}/Ga^{3+}/Ge^{4+}$ and In^{3+}/Sn^{4+} species, it was shown, that indeed the catalytic selectivity of In_2O_3 and SnO_2 towards CO_2 is very pronounced. In contrast, both Ga_2O_3 and GeO_2 are less CO_2 selective but their overall reaction profiles are very similar. Considering this MSR selectivity we might also anticipate a different activity of SnO_2 and GeO_2 in the (reverse) water-gas shift reaction, which in the case of Ga_2O_3 additionally accounted for the lowering of the CO_2 selectivity [8]. Above all, the MSR behaviour of SnO_2 and GeO_2 also raises interesting questions about the activity and selectivity of the corresponding oxide-supported Pd catalysts in MSR. For Pd/Ga_2O_3, the introduction of Pd and the subsequent reductive formation of specific Pd-Ga bimetallic phases yielded an almost complete suppression of CO formation and, in turn, a very pronounced CO_2 selectivity. A similar observation was made on the Pd/In_2O_3 catalyst, although here the situation is complicated by the already high CO_2-selectivity of the pure oxide. It is therefore interesting to study if and how the eventual formation of specific Pd-Sn and Pd-Ge bimetallic phases influences and changes the MSR activity and selectivity of the respective clean oxides.

Acknowledgements

We thank the FWF (Austrian Science Foundation) for financial support under project P20892-N19. The authors acknowledge support from the European Union under the Framework 6 program under a contract from an Integrated Infrastructure Initiative (Reference 026019 ESTEEM). We also thank Frederik Klauser from the Institute of Physical Chemistry, University of Innsbruck, for assistance with X-ray photoelectron spectroscopy.

References

[1] M. Batzill, U. Diebold, Prog. Surf. Sci. 79 (2005) 47-154
[2] A. Neramittagapong, S. Hoshino, T. Mori, J. Kubo, Y. Morikawa, Chem. Lett. (2002) 1078-1079
[3] C. Wöll, Prog. Surf. Sci 82 (2007) 55-120
[4] S. Penner, H. Lorenz, W. Jochum, M. Stöger-Pollach, D. Wang, C. Rameshan, B. Klötzer, Appl. Catal. A 358 (2009) 193-202 and references therein
[5] H. Lorenz, W. Jochum, B. Klötzer, M. Stöger-Pollach, S. Schwarz, K. Pfaller, S. Penner,Appl. Catal. A 347 (2008) 34-42 and references therein
[6] T. Mori, S. Hoshino, A. Neramittagapong, J. Kubo, Y. Morikawa, Chem. Lett. (2002) 390
[7] T. Shido, Y. Iwasawa, J. Catal. 140 (1993) 575-584
[8] W. Jochum, S. Penner, R. Kramer, K. Föttinger, G. Rupprechter, B. Klötzer, J. Catal. 256 (2008) 278-286
[9] T. Hara, Y. Nakamura, J. Nishimura, Appl. Catal. A 341 (2008) 65-69
[10] H. Lorenz, Q. Zhao O. I. Lebedev, S. Turner, G. Van Tendeloo, B. Klötzer,C.Rameshan, S. Penner, submitted
[11] R. J. Meyer, Gmelins Handbuch der Anorganischen Chemie, 8. Auflage, 1958, Verlag Chemie, GmbH Weinheim/Bergstrasse
[12] J. F. Sarver, F.A. Hummel, J. Electrochem. Soc. 108 (1961) 195-196
[13] R. Schwarz, E. Haschke, Z. Anorg. Chemie 252 (1943) 170-172
[14] S. Penner, H. Lorenz, W. Jochum, M. Stöger-Pollach, D. Wang, C. Rameshan, B. Klötzer, Appl. Catal. A 358 (2009) 203-210 and references therein
[15] W. H. Baur, A. A. Khan, Acta Crystallogr. B, 27 (1971) 2133-2139
[16] F. Izumi, J. Solid State Chem. 38 (1981) 381-385
[17] M. S. Moreno, R. F. Egerton, J. J. Rehr, P. A. Midgley, Phys. Rev. B 71 (2005) 035103-1 - 035103-6
[18] J. A. Lee, G. V. Raynor, Proc. Phys. Soc., London 67 (1954) 737-747
[19] H. Bitterer, Gmelins Handbuch der Anorganischen Chemie, Zinn Teil C1, 8. Auflage, 1972, Verlag Chemie, GmbH Weinheim/Bergstrasse and references therein
[20] L. Bertini, P. Ghigna, M. Scavini, F. Cargnoni, Phys.Chem.Chem.Phys. 5 (2003) 1451-1456
[21] A. F. Hollemann, N. Wiberg, Lehrbuch der Anorganischen Chemie, 102. Auflage 2007, Walter de Gruyter, Berlin, New York
[22] J.M. Tatibouet, Appl. Catal. A, 148 (1997) 213-252
[23] M. Badlani, I. E. Wachs, Catal. Lett. 75 (2001) 137-149